Arsenic (V) Removal by an Adsorbent Material Derived from Acid Mine Drainage Sludge

Erdenechimeg Byambaa [1], Jaeyoung Seon [1], Tae-Hyun Kim [1], Shin Dong Kim [2], Won Hyun Ji [3] and Yuhoon Hwang [1,*]

[1] Department of Environmental Engineering, Seoul National University of Science and Technology, Seoul 01811, Korea; chimgee8606@gmail.com (E.B.); 19512038@seoultech.ac.kr (J.S.); th.kim@seoultech.ac.kr (T.-H.K.)

[2] E&Chem Solution Co., Ltd., Gyeonggi-do 11154, Korea; catalite@hanmail.net

[3] Mine Reclamation Corp. Research Center, Gangwon-do 26464, Korea; greenidea@mireco.or.kr

* Correspondence: yhhwang@seoultech.ac.kr; Tel.: +82-2-970-6626

Abstract: Arsenic is a toxic element that is often found in drinking water in developing countries in Asia, while arsenic poisoning is a serious worldwide human health concern. The objective of this work is to remove arsenic (V) (As(V)) from water by using an adsorbent material prepared from mine waste, called MIRESORB^{TM}, which contains Fe, Al. The performance of the MIRESORB^{TM} adsorbent was compared with granular ferric hydroxide (GFH), which is a commercial adsorbent. Adsorbents were characterized by using scanning electron microscopy (SEM), X-ray fluorescence spectroscopy (XRF), X-ray diffractometry (XRD), and N_2 sorption with Brunauer–Emmett–Teller (BET) analysis. The kinetics, isotherms, and pH-dependency of arsenic adsorption were interrogated to gain insights into arsenic adsorption processes. The maximum adsorption capacity of MIRESORB^{TM} was 50.38 mg/g, which was higher than that of GFH (29.07 mg/g). Moreover, a continuous column test that used environmental samples of acid mine drainage was conducted to evaluate the MIRESORB^{TM} material for practical applications. The column could be operated for more than 5840 bed volumes without a breakthrough. Successful operation of a pilot plant using MIRESORB^{TM} adsorbent was also reported. Thus, these studies demonstrate MIRESORB^{TM} as a highly efficient and economical adsorbent derived from recycled mine sludge waste.

Keywords: arsenic removal; arsenate; granular ferric hydroxide; mine waste adsorbent

1. Introduction

Arsenic exists as oxides in the soil, sediment, and water in many parts of the world and originates from both natural and anthropogenic activities. Arsenic (V) (As(V)) is the predominant species under oxidizing conditions, specifically as oxyanions of arsenic acid (H_3AsO_4, $H_2AsO_4^-$, $HAsO_4^{2-}$, and AsO_4^{3-}), while arsenic (III) (As(III)) exists as arsenious acid (H_3AsO_3, $H_2AsO_3^-$, and $HAsO_3^{2-}$) under mildly reduced conditions [1]. Arsenic presents a high danger to human health when present in drinking water and, as such, toxicity related to arsenic is a severe concern worldwide. Arsenic compounds are recognized as Group 1 carcinogens by the International Agency for Research on Cancer (IARC) [2]. The World Health Organization currently recommends a maximum contaminant level (MCL) of arsenic in drinking water of 10 μg/L [3]. In Korea, the standard for arsenic in drinking water has been set at 10 μg/L, with 50 μg/L as the maximum allowable concentration in rivers and lakes as regulated by ambient water quality standards [4].

Arsenic pollutants are prevalent in developing countries such as Argentina, Chile, China, Mongolia, Nepal, and other Southeast Asian countries [5]. In recent years, 94% of Asian regions have a risk of arsenic contamination in excess of 10 μg/L in drinking water from wells and, in some countries, concentrations reach more than 50 μg/L [6]. The mining sector, in particular, is the primary anthropogenic source of arsenic contamination. Acid

mine drainage (AMD) is the runoff produced, when water contacts exposed rocks that contain sulfur-bearing minerals, which react with water and air to form sulfuric acid and dissolved iron [7]. This acidic runoff dissolves heavy metals such as arsenic, which pollute ground and surface water.

Mining in areas with scarce water resources presents many problems. In these cases, it is necessary to evaluate drinking water for toxic contaminants and mitigation techniques to remove any heavy metals. For example, ground and surface water pollution in Mongolia has been relatively poorly studied and arsenic pollution is anticipated to increase due to mining activities [8]. During the mining season, the major rivers in northern Mongolia become polluted by heavy metals such as Mn, Al, Cd, and As [9]. Separately, in Korea, many abandoned metal mines have been improperly managed, and environmental issues continuously emerge in the areas' nearby closed mines [10].

A wide range of technologies can remove arsenic from water, such as membrane separation, ion exchange, coagulation, precipitation, and adsorption [11,12]. Among the many techniques currently available for removing arsenic from water, adsorption is considered to be one of the most promising because of the low cost, high efficiency, and ease of operation [13,14]. Many studies have exploited zeolite, chitosan, granular ferric hydroxide (GFH), and other materials as adsorbents to remove arsenic [15,16]. Iron-based adsorbents have attracted much interest due to their high efficiency in arsenic remediation, environmental friendliness, and abundance on earth [11]. Extensive studies have been conducted on iron-containing adsorbents with high affinities for arsenic species. Iron-containing oxides have high surface activities due to surface hydroxylation and ionization under certain medium conditions, which vary surface charge [17].

We aimed to develop an iron-based adsorbent from waste materials. Large quantities of sludge are generated during AMD treatment processes, and this waste material consists of amorphous micron- and submicron-sized metal oxide/hydroxide particles with high specific surface areas [18,19]. The most abundant elements in AMD sludge are Fe and Al, which are known to effectively remove arsenic [15,20]. Thus, we anticipate that sludge would have high potential for arsenic adsorption.

In this study, an iron-based adsorbent called MIRESORB$^{\text{TM}}$ was prepared from coal mine drainage sludge, a byproduct of coal mine drainage treatments. The performance of MIRESORB$^{\text{TM}}$ was compared with that of a commercially available adsorbent, GFH. Adsorbents were characterized by scanning electron microscopy (SEM), X-ray fluorescence spectrometry (XRF), X-ray diffractometry (XRD), and N$_2$ sorption with Brunauer–Emmett–Teller (BET) analysis. Lab-scale batch experiments probed the adsorption kinetics, isotherms, and pH-dependence of arsenic by the adsorbent materials. Moreover, continuous column tests that used environmental samples of acid mine drainage were conducted at lab- and pilot-scales to establish the practical application of the MIRESORB$^{\text{TM}}$ adsorbents.

2. Materials and Methods

2.1. Materials

The MIRESORB$^{\text{TM}}$ adsorbent was supplied by E&Chem Solution Co., Ltd. (Pocheon-si, Korea) and was prepared by using acid mine drainage sludge. The initially pellet-shaped adsorbent was ground and sieved to prepare adsorbent particles 150 μm in size. The adsorption behaviors of the sludge-based adsorbent material were compared with those of commercially available GFH (GEH$^®$ 102, GEH Wasserchemie GmbH, Osnabrück, Germany) adsorbents. Sea sand (30–50 mesh, Samchun, Seoul, Korea) was used as an inert column filling material.

Analytical grade HCl (Daejung chemicals and metals, Siheung-si, Korea), NaOH (Samchun, Seoul, Korea), and NaNO$_3$ (Duksan pure chemicals, Ansan-si, Korea) were purchased and used without further purification. The As(V) stock solution was prepared by using dibasic sodium arsenate (Na$_2$HAsO$_4$·7H$_2$O) purchased from Wako pure chemical (Osaka, Japan). All solutions were prepared by using deionized (DI) water (>18 MΩ·cm) (Milli-Q$^®$ Reference Water Purification System, Merck, Darmstadt, Germany).

2.2. Characterization

Adsorbents were characterized by using a scanning electron microscope (SEM, VEGA3, Brno, Tescan, Czech Republic), X-ray fluorescence spectrometers (XRF, ARL QUANT'X, Thermo fisher scientific, Waltham, MA, USA), and X-ray diffractometers (XRD, DE/D8 Advance, Bruker, Germany). A Brunauer–Emmett–Teller (BET) surface area analyzer (3flex, Micromeritics, Norcross, GA, USA) was used to establish the specific surface area of the adsorbents. The concentrations of arsenic and iron in aqueous solution were determined by inductively coupled plasma atomic emission spectrometry (ICP-AES, 5110 SVDV, Agilent, Singapore). Arsenic content in the fresh and spent adsorbents was determined by a microwave digestion system (Multiwave 7000, Anton Paar GmbH, Graz, Austria). The point of zero charge (pH_{PZC}) of adsorbent samples was determined by measuring the pH change of an $NaNO_3$ solution after adding the adsorbent, as described in [17]. Solution pH was determined by a pH meter (NeoMet, Istek Inc., Seoul, Korea).

2.3. Arsenic Adsorption Batch Test

2.3.1. Adsorption Kinetic

The kinetics of arsenic adsorption was evaluated by a batch test with a 30 mg/L initial concentration of As(V). First, 100 mL of an aqueous solution containing 30 mg/L As(V) was poured into a beaker, and the pH was adjusted to 6.0 by adding 0.1 M HCl and NaOH. Then, 0.1 g of adsorbent material was added to this 100 mL solution and the solution was stirred continuously. Subsequently, 3 mL samples were collected at 1, 3, 6, 24, 48, 72, 120, and 168 h for analysis. Samples were filtered by using a polyethersulfone (PES) membrane filter (0.2 μm, Hyundai micro Co. Ltd. (Seoul, Korea) and arsenic content was determined as described above.

The adsorption capacity of arsenic was obtained by using Equations (1) and (2) below:

$$q_e = (C_0 - C_e) \times V/M \tag{1}$$

$$\% \ Removal = (C_0 - C_e)/C_0 \times 100 \tag{2}$$

where C_0 is the initial concentration of arsenic (mg/L), C_e is the equilibrium concentration of arsenic (mg/L), m is the mass of adsorbent (g), and V is the volume of the solution (L).

The adsorption kinetics were evaluated by applying the following kinetic equations, i.e., pseudo-first-order (Equation (3)) and pseudo-second-order (Equation (4)) [21] as follows:

$$q_t = q_e \left(1 - e^{-k_1 t}\right) \tag{3}$$

$$q_t = \frac{k_2 q_e^2 t}{1 + k_2 q_e t} \tag{4}$$

where q_t is the adsorbed amount of arsenic at time t (mg/g), q_e is the equilibrium concentration of arsenic (mg/g), k_1 is the first-order rate constant (1/h), and k_2 is the second-order rate constant (g/mg·h).

2.3.2. Adsorption Isotherm

Adsorption isotherms were determined through adsorption experiments with the same 50 mg/L initial concentration of As(V) but different adsorbent doses. Then, 50 mL of the arsenic-containing aqueous solution was placed into conical centrifuge tubes, and the pH was adjusted to 6.0 by adding 0.1 M HCl and NaOH. Adsorbents were added to the solution at doses ranging from 0.0025 to 0.5 g/L. Conical tubes were continuously stirred at 20 rpm by using a vertical stirrer. After 48 h, the solution was filtered with a PES filter. Arsenic concentrations were determined as described above.

Adsorption isotherm data were fitted as a Langmuir isotherm (Equation (5)) and Freundlich isotherm (Equation (6)) [22,23] as follows:

$$q_e = q_m \frac{a_L C_e}{1 + a_L C_e} \tag{5}$$

$$q_e = K_F C^{1/n} \tag{6}$$

where q_e is the quantity of the arsenic adsorbate adsorbed per unit weight of solid adsorbent, q_m is the maximum sorption capacity of the adsorbent (mg/g), C_e is the equilibrium concentration of the adsorbate in solution (mg/L), and a_L is the Langmuir affinity constant. The constants K_F and $1/n$ reflect the adsorption capacity and adsorption intensity, respectively, of the adsorbent.

2.3.3. Effect of pH

The influence of pH (3–10) on arsenic adsorption was evaluated following an experimental procedure similar to that described in Section 2.3.1. The initial concentrations of arsenic and adsorbent dosage were 30 mg/L and 0.5 g/L, respectively. The pH was adjusted to the desired level by adding 0.1 M HCl and NaOH. Conical tubes were continuously stirred at 20 rpm by using a vertical stirrer. After 48 h, the solution was filtered with a PES filter. Arsenic concentrations were determined as described above.

2.3.4. Adsorption from Environment Samples of Acid Mine Drainage

The capacity of the adsorbent to extract arsenic from an environmental sample of acid mine drainage (AMD) was evaluated. Acid mine drainage was collected from a mine drainage collection facility located in a gold mine. The AMD contained 291 ± 19 µg/L of As, 871 ± 102 µg/L of Zn, 210 ± 50 µg/L of Cd, and 65 ± 8.7 µg/L of Fe.

An arsenic stock solution was mixed with the environmental sample of AMD to achieve an initial arsenic concentration of 50 mg/L. Then, 2.5 mL of aqueous solution containing 1000 mg/L of As(V) was added to 47.5 mL AMD. The pH was adjusted to 6.0 by adding 0.1 M HCl and NaOH. Then, 0.05 g of adsorbents were added to this 50 mL solution, reflecting a 1 g/L dosage of adsorbent. A solution sample was taken at 48 h, and arsenic concentrations were determined as described in Section 2.2.

2.4. Continuous Column Test

2.4.1. Lab-Scale Test

The adsorption column experiments were conducted at room temperature using a glass column with a 1.5 cm inner diameter and 20 cm length (Figure S1). Sea sand was used as an inert layer to fill the top and bottom 5 cm of the column, and either GFH or MIRESORB™ were placed in the 10 cm between the sand layers. Flowrate was controlled by a peristaltic pump at 1.2 mL/min, which provided an empty bed contact time (EBCT) of 11.8 min. The environmental samples of AMD were filtered by a 47 mm glass microfiber filter (GF/C, 1.2 µm, Whatman, Kent, UK) before use in column tests. The pH of AMD was around 7.5.

2.4.2. Pilot-Scale Test

A pilot plant was installed near an abandoned gold mine in Korea to treat mine drainage. The total volume of the adsorption bed was 90 L, and the width, length, and depth were 800 mm, 350 mm, and 320 mm, respectively. The adsorption bed was filled with 30 kg of the MIRESORB™ adsorbent, and the filling volume was 50 L. Pelletized adsorbent that had not been ground was used in the pilot plant; mine drainage was injected; therefore, the EBCT was between 18 and 500 min. Samples prior to and following adsorption were collected and analyzed for As.

3. Results and Discussion

3.1. Adsorbent Characterization

Powder X-ray diffractometry (PXRD) was used to probe the crystal structures of the adsorbents of powdered GFH and MIRESORB™. The XRD patterns of both adsorbent materials are shown in Figure 1. According to the manufacturer, GFH consists of akageneite (β-FeO(OH)) and iron hydroxide (Fe(OH)$_3$). The PXRD pattern of GFH clearly shows a diffraction pattern that corresponds to akageneite [24], while patterns attributed to iron hydroxide could not be resolved due to overlapping peak positions with akageneite (Figure 1). By comparison, the PXRD pattern of MIRESORB™ shows only weak diffraction peaks originating from iron hydroxide [25]. The diffraction patterns of both GFH and MIRESORB™, however, exhibit low peak intensities that reflect low crystallinity. The PXRD analyses establish that the GFH and MIRESORB™ predominantly consist of akageneite and iron hydroxide, respectively.
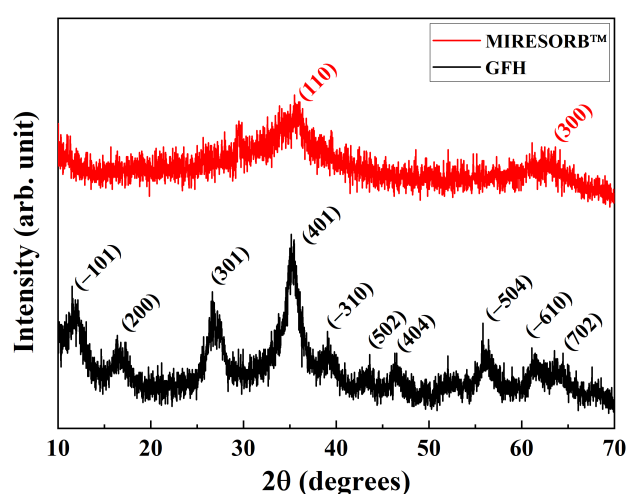
Figure 1. Powder X-ray diffractogram of granular ferric hydroxide (GFH) (**black line**) and MIRESORB™ (**red line**).

Scanning electron microscope images of the grains and grain surfaces of MIRESORB™ and GFH are displayed in Figure S2. The surfaces of both samples have large grain sizes and are rough because of fine particles attached to the grain surface. Interestingly, the GFH adsorbent had smaller fine particles than MIRESORB™, which may influence the surface area.

The elemental compositions of the adsorbents were estimated by XRF analysis, as summarized in Table 1. Iron is the most abundant element in GFH and MIRESORB™ and accounts for the crystalline phases observed in the PXRD patterns. The GFH has a higher iron content of 93.0% versus the 78.1% iron content in MIRESORB™. Magnesium and aluminum are minor elements in GFH adsorbents. MIRESORB™ contains a broader range of elements, which can vary because the composition of the precursor sludge depends on the source of mine drainage [19]. The composition of MIRESORB™ includes Fe (78.1%), Al (9.20%), Ca (5.73%), and Mg (4.0%), which are the major constituents of AMDS. These analyses indicate that MIRESORB™ materials have high amounts of iron oxide and low Ca, Si, Al, and Mn contents.

Table 1. Elemental compositions estimated by X-ray fluorescence spectrometry.

Adsorbent	Mg	Al	Si	Ca	Fe	Ni	Zn
MIRESORB™	4.00	9.20	1.92	5.73	78.1	0.12	0.12
GFH	4.40	2.19	0.15	0.15	93.0	ND	ND

Note, elemental composition less than 0.05% was regarded as ND.

The specific surface area (SSA) and pore area are important factors for adsorption and were estimated for the MIRESORB[TM] and GFH by analyzing N_2 adsorption/desorption isotherms by using the BET method (Figure 2). The SSAs of powdered MIRESORB[TM] and GFH were established as 233 and 306 m^2/g, respectively (Table 2). The GFH exhibits approximately 24% higher SSA than MIRESORB[TM], which is due to the smaller fine particles on the surface, as evidenced by SEM images (Figure S2). As shown in Figure 2a, the N_2-adsorption isotherms of GFH and MIRESORB[TM] have different types of hysteresis loops, namely, type II and type IV for MIRESORB[TM] and GFH, respectively. This indicates that MIRESORB[TM] adsorbents likely have a macropore structure and promote unrestricted mono-multilayer adsorption as compared with the type IV hysteresis of GFH, provides evidence of capillary condensation in mesopores [26]. The pore volume and pore size of the adsorbents were estimated by the Barrett, Joyner, Halenda (BJH) method and are summarized in Table 2. The pore volume was calculated to be 0.33 cm^3/g for GFH materials and 0.57 cm^3/g for MIRESORB[TM] materials. Moreover, the pore volume distribution graph shows that MIRESORB[TM] materials have a larger fraction of pores with diameters over 10 nm (Figure 2b). The pore sizes in MIRESORB[TM] materials are also approximately 66% larger than that for GFH materials. Notably, MIRESORB[TM] materials have approximately 24% smaller surface areas than GFH materials, but the nearly 72 and 66% larger pore volume and size of these materials, respectively, might lead to high As(V) adsorption efficacy.
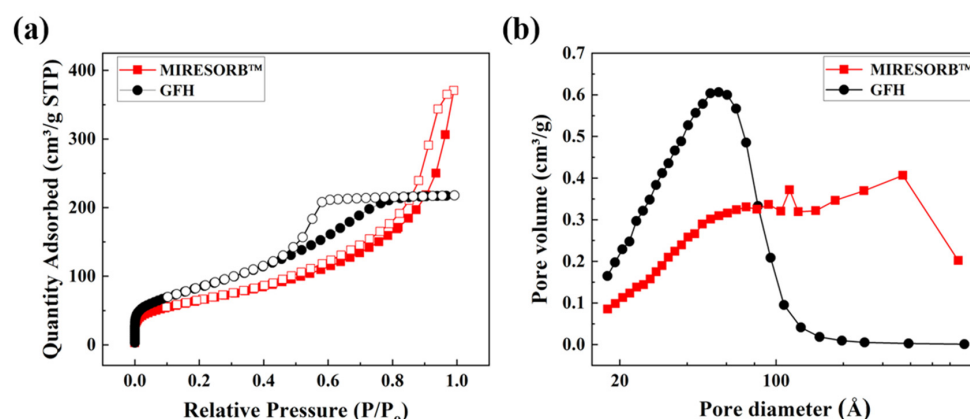

Figure 2. (**a**) N_2 adsorption/desorption isotherm; (**b**) The Barrett, Joyner, Halenda (BJH) pore volume distributions, for GFH and MIRESORB[TM] materials.

Table 2. Surface areas, pore volumes, and pore sizes of the adsorbent materials.

Characteristic	MIRESORB[TM]	GFH
Surface area (m^2/g)	233	306
Pore volume (cm/g^3)	0.57	0.33
Pore size (nm)	7.30	4.39

3.2. Adsorption Kinetics

The equilibration time is critical for designing efficient adsorption systems because it influences construction, operating, and maintenance cost, which are considerations in selecting processes for drinking water treatment [27]. Adsorption kinetics are also important for additional isotherm testing because the kinetic tests could identify the time for achieving equilibrium. Figure 3 shows kinetic plots of As(V) adsorption on MIRESORB[TM] and GFH materials. The initial adsorption rate was generally rapid and was followed by slower adsorption. The GFH material adsorbed 50% of its total capacity in 6.7 h, while the MIRESORB[TM] material only required 2.5 h to reach 50% capacity. Equilibrium was reached after 24 h and 48 h for the MIRESORB[TM] and GFH materials, respectively.

(**a**) (**b**)
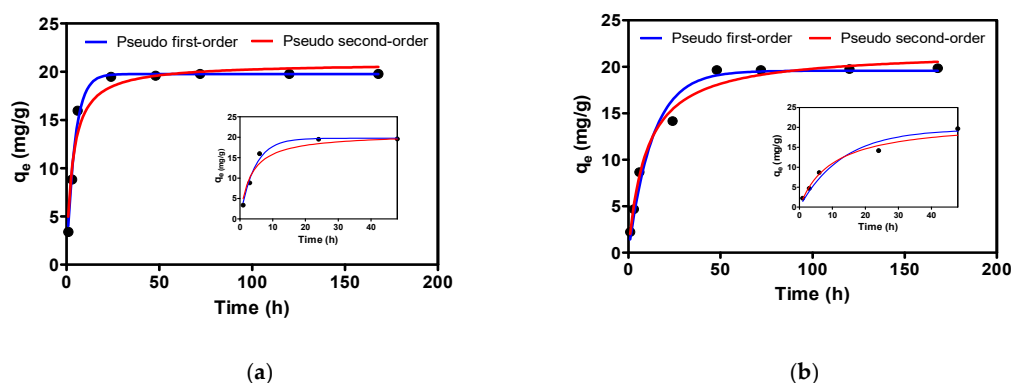
Figure 3. Arsenic adsorption kinetics. (**a**) MIRESORB^{TM}; (**b**) GFH. The initial arsenic (V) (As(V)) concentration was 30 mg/L, the adsorbent dose was 1 g/L, the pH was 6.0, and the contact times were 1, 3, 6, and 24 h and 2, 3, 5, and 7 d.

The data of arsenic removal from solution were used to estimate arsenic adsorption kinetics by fitting of the pseudo-first-order (PFO, Equation (3)) kinetic model and the pseudo-second-order (PSO, Equation (4)) kinetic model. Rate constants from this fitting analysis are tabulated in Table 3. The q_e values for the MIRESORB^{TM} and GFH were similar, but the kinetic constants differed substantially. The kinetic constants for GFH were 0.076 h^{-1} and 0.005 g/mg·h based on the PFO and PSO models. The kinetic constants for MIRESORB^{TM} were approximately three times higher; namely, the constant for the PFO was 0.227 h^{-1} and for the PSO was 0.015 g/mg·h. Similar trends were observed for adsorption capacity, which is described in the following isotherm section. The kinetic parameters positively correlated with the pore volumes of the adsorbent (Table 1). The rapid As(V) adsorption kinetics of the MIRESORB^{TM} adsorbent were attributed to the large pore volumes versus GFH.
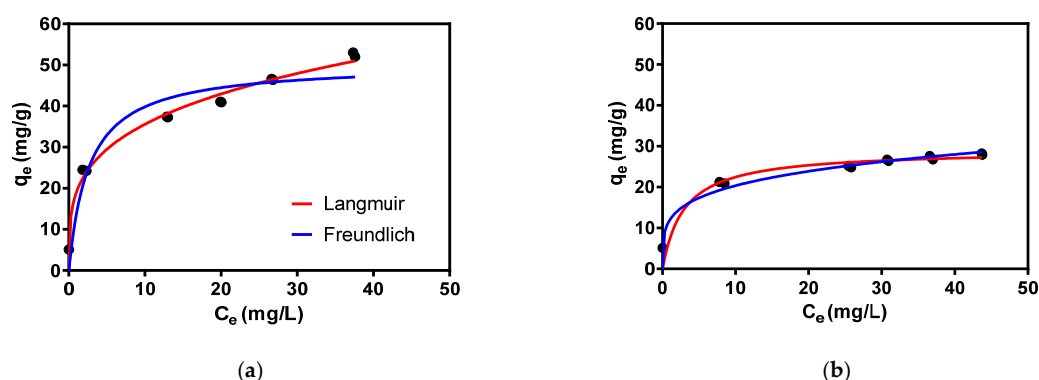
Table 3. Kinetic parameters for As(V) adsorption by MIRESORB^{TM} and GFH materials.

Adsorbent	Pseudo First-Order			Pseudo Second-Order		
	q_e (mg/g)	k_1 (1/h)	R^2	q_e (mg/g)	k_2 (g/(mg·h))	R^2
MIRESORB^{TM}	19.76	0.227	0.990	20.88	0.015	0.958
GFH	19.58	0.076	0.977	21.74	0.005	0.986

3.3. Adsorption Isotherm

Isotherm studies are useful for quantifying adsorption capacity. Generally, Langmuir and Freundlich isotherm models are employed to fit experimental data, and the results are used to describe interactions between adsorbate and adsorbent [28].

The arsenic sorption plots for the MIRESORB^{TM} and GFH materials were fitted by Langmuir and Freundlich isotherms (Figure 4). The parameters and correlation coefficients are given in Table 4. The data were fitted more accurately by the Freundlich isotherm than the Langmuir isotherm, indicating multilayer adsorption of arsenic on a heterogeneous surface [29]. This type of adsorption is expected for MIRESORB^{TM} adsorbents, which have several adsorption sites, including iron oxide, iron (oxy)hydroxide, and other metal oxides. The 1/n values for As(V) adsorption on both adsorbents (MIRESORB^{TM} = 0.27 and GFH = 0.23) establish favorable adsorption.

(a)　　　　　　　　　　　　　　　　　　　　　　　　(b)

Figure 4. Arsenic isotherm materials. (**a**) MIRESORB^{TM}; (**b**) GFH. The initial As(V) concentration was 50 mg/L, the adsorbent dose was 0.01–10 g/L, the pH was 6.6, and the contact time was 48 h.

Table 4. Isotherm parameters for As(V) adsorption to MIRESORB^{TM} and GFH materials.

Adsorbent	Langmuir Isotherm			Freundlich Isotherm		
	q_m (mg/g)	K_L (L/mg)	R^2	K_F ([mg/g]·[mg/L]$^{1/n}$)	n (1/n)	R^2
MIRESORB^{TM}	50.38	0.38	0.91	19.04	3.68 (0.27)	0.98
GFH	29.07	0.33	0.94	12.00	4.35 (0.23)	0.95

Fitting by the Langmuir model provides maximum As(V) adsorption capacities (q_m) for MIRESORB^{TM} and GFH of 50.38 mg/g and 29.07 mg/g, respectively. The q_m for the MIRESORB^{TM} was higher than that reported in similar previous studies of AMDS, in which the As(V) adsorption capacity of AMDS was approximately 10–70 mg/g and varied with AMDS characteristics and experimental conditions [29–31]. A composite AMDS with organic binder material showed slightly decreased adsorption capacity. Lee et al. (2015) reported that bead type adsorbents that employed AMDS with alginate had a q_m for As(V) of 21.8 mg/g [18]. The AMDS coated with polyurethane have shown a q_m of 7.3 mg/g [15]. MIRESORB^{TM} is an adsorbent prepared by using byproducts from coal mines. Thus, the high adsorption capacity of MIRESORB^{TM} for As(V) is a good indicator of its suitability for removing As(V) from contaminated water.

3.4. Effect of pH

The pH is a critical variable in environmental studies as it influences both the surface chemistry of the adsorbent and speciation of the adsorbate [32]. The adsorption of As(V) onto MIRESORB^{TM} and GFH was interrogated over a pH range of 3 to 10, which are shown in Figure 5a. The adsorption capacity of both adsorbents decreased with increasing pH and ranged from 6.3–56.8 mg/g for GFH adsorbents and from 27.6–77.8 mg/g for MIRESORB^{TM} adsorbents for pH conditions from 3–10. Overall, the MIRESORB^{TM} materials had higher adsorption capacities over all of the tested pH conditions. The pH$_{pzc}$ of both adsorbents are presented in Figure 5b. The pH$_{pzc}$ of the MIRESORB^{TM} and GFH materials were 8.7 and 6.2, respectively. Thus, the MIRESORB^{TM} materials would be positively charged over a wider pH range (up to pH of 8.7) versus GFH (up to pH of 6.2).

(**a**)　　　　　　　　　　　　　　　　　　　(**b**)
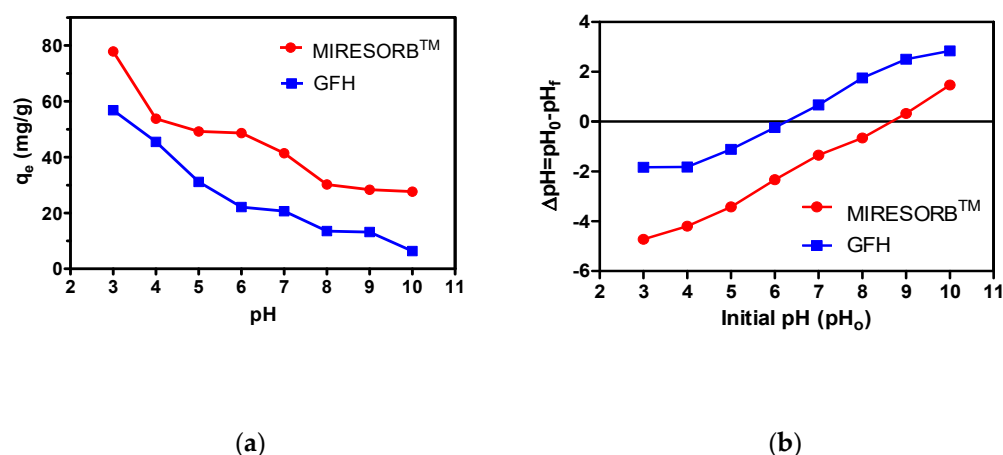
Figure 5. (**a**) Influence of pH on the arsenic adsorption capacity of MIRESORB[TM] and GFH materials. The initial As(V) concentration was 30 mg/L, the adsorbent dose was 0.5 g/L, the contact time was 48 h. (**b**) Point-of-zero charge determination for the MIRESORB[TM] and GFH materials.

The solution pH influences the arsenic adsorption by influence adsorbent surface charge and speciation of arsenic ions. The valence of As(V) species changes from -1 to -3 as pH increases (pK = 2.2, 6.98, and 11.6), due to the deprotonation of species such as $H_2AsO_4^-$, $HAsO_4^{2-}$, and AsO_4^{3-}. Simultaneously, the surface charge of the adsorbent becomes negative under high pH conditions due to deprotonation of the adsorbent surface. In iron oxides, the $FeOH^+$ groups predominate at pH conditions lower than the pH_{pzc} of iron oxide, and FeO^- groups predominate at pH conditions higher than this pH_{pzc} [33]. Under high pH conditions, arsenic adsorption to iron oxides is inhibited by electric repulsions or competitions with other anions, such as hydroxyl ions [29,32,33]. Thus, the quantity of adsorbed As(V) is maximal under acidic pH conditions, which agrees well with experimental results. Adsorption under alkaline pH conditions could originate from coordination complex adsorption [34].

Since the MIRESORB[TM] materials would be positively charged over a wider pH range (up to pH of 8.7), therefore, the MIRESORB[TM] materials would be expected to have greater As(V) adsorption performance over a wide range of pH.

3.5. Practical Applicability of Adsorbent

3.5.1. Treatment of an Environmental Acid Mine Drainage Sample

The As(V) adsorption performance from an environmental sample of AMD was evaluated and compared with that As(V) adsorption from DI water (Figure S3). While aqueous solutions of As(V) in DI water were used for experiments in Sections 3.2–3.4, adsorption experiments, here, were performed with an As(V)-containing AMD sample collected from a gold mine. The AMD contained several heavy metals such as Zn, Cd, and Fe; therefore, the competitive adsorption should be examined. The removal efficiency of As(V) from the environmental AMD sample was nearly the same as from DI water. For example, the MIRESORB[TM] and GFH materials removed 74.7 and 66.9% of As(V), respectively, while 77.7 and 69.2% of removal efficiencies were achieved from the DI water cases. Nonetheless, the difference is not significant. This demonstrates that these adsorbents could be applied for AMD treatment without significant inhibition effects.

3.5.2. Lab-Scale Column Study

A continuous adsorption experiment was conducted to evaluate the MIRESORB[TM] and GFH adsorbents for practical applications as a water filtration material for arsenic removal. The environmental AMD sample collected from the gold mine was used as a feed solution, which contained As at 270–350 µg/L, Zn 250–1000 µg/L, Cd 40–260 µg/L, and

had a pH in the range of 7.3–7.7. The flow rate was set to 1.2 mL/min, which resulted in an empty bed contact time of 11.8 min.

The columns operated up to 5840 bed volume (BV) without apparent breakthrough for both adsorbent materials (Figure 6). The As concentration in the effluent was generally less than 10 μg/L, which met the WHO drinking water standard. The As concentration in the effluent exceeded 10 μg/L in a few samples; however, the As concentration was still lower than 50 μg/L, which was the same as the regulated concentration specified by Korea for water in the environment. The maximum As concentration in the effluent was 20 and 30 μg/L for MIRESORB^{TM} and GFH, respectively. This indicates that the adsorption by the AMDS derived adsorbent, MIRESORB^{TM}, is an effective solution for treating As-contaminated wastewater such as mine drainage.
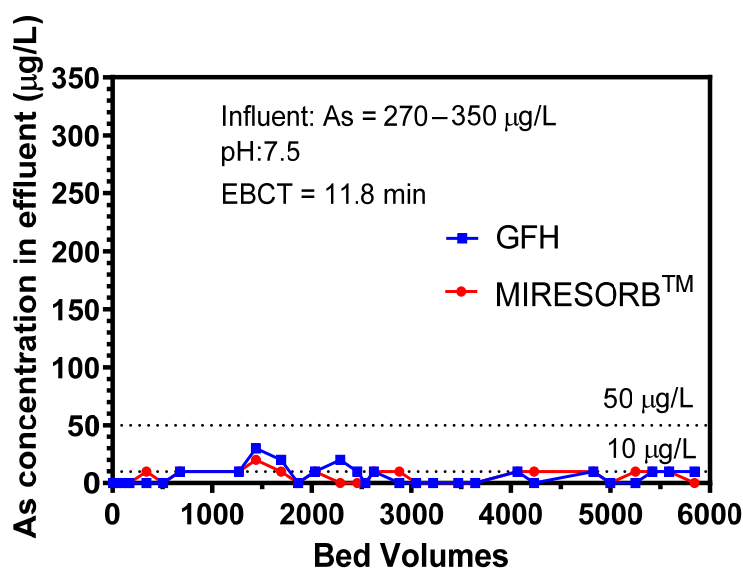

Figure 6. Results from lab-scale column experiments of arsenic adsorption by MIRESORB^{TM} and GFH adsorbents.

The spent adsorbent from the column experiments was analyzed for adsorbed arsenic. The sample was subjected to an acid digest assisted by microwaves, and the arsenic in the sample was determined by ICP-AES. The arsenic concentration in the spent MIRESORB^{TM} and GFH was 0.052% and 0.020%, respectively as compared with the arsenic concentration in the fresh adsorbent which was less than 0.001%, establishing substantially higher arsenic content in the spent adsorbent than the fresh adsorbent.

The SEM/EDS images of fresh and spent adsorbents are presented in Figures S4 and S5. The morphology was not changed during the column experiments, but the elemental composition obtained by EDS showed different results. On the one hand, the fresh GFH and MIRESORB^{TM} consisted of Fe, O, Al, and C, similar to the composition obtained by XRF. On the other hand, As was detected in spent adsorbents, the wt.% of As was 0.41% for GFH and 1.86% for MIRESORB^{TM}. The higher wt.% was obtained in the EDS analysis because it analyzed the elemental composition at the surface. This data unambiguously establishes that both materials adsorb arsenic during the column experiments.

3.5.3. Pilot-Scale Study

A pilot-scale adsorption experiment using the MIRESORB^{TM} adsorbent was conducted to investigate the applicability of this adsorbent for the practical treatment of mine drainage, the results of which are presented in Figure 7. The arsenic concentration in the feed varied from 350–410 μg/L during the first week of operation but remained stable at around 120–130 μg/L over the following three weeks. An EBCT of 18.5 min was used for the first five days of operation, but the arsenic removal efficiency was less than 50%

under these conditions. Then, the EBCT was increased to 100 min, which boosted the As removal efficiency to around 60%. Further increasing the EBCT to 170 min and 500 min raised the As removal efficiency. The removal efficiency gradually increased throughout the one-month experiment, with more than 90% removal efficiency during the last week of operation. The arsenic concentration in the effluent was less than 10 μg/L during the last week and less than 50 μg/L over the final three weeks of operation, when the EBCT was more than 170 min. This demonstrates that, under proper operating conditions, the MIRESORB[TM] absorbent could be deployed in a mine drainage treatment system.
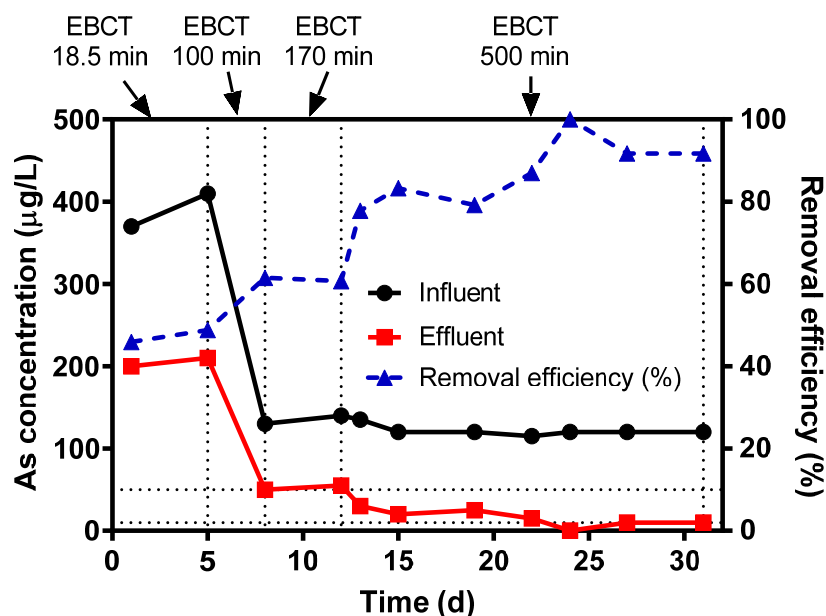
Figure 7. Results from pilot-scale experiments of arsenic removal by using MIRESORB[TM] as an adsorbent material.

4. Conclusions

Arsenic pollutants are prevalent in developing countries. Thus, locally available and low-cost adsorbent materials are promising technological solutions for arsenic removal for water treatment at the local level. This study evaluated the physical characteristics and arsenic adsorption performances of new MIRESORB[TM] adsorbent materials that were derived from iron-rich acid mine drainage sludge. The materials were also compared with commercially available adsorbent GFH. The specific surface area, pore volume, and pore size of powdered MIRESORB[TM] were 233.48 m^2/g, 0.57 cm/g^3, and 7.30 nm, respectively. While the surface area of the MIRESORB[TM] absorbent was lower than GFH, the relatively larger pore openings supported more efficient mass transport of aqueous arsenic, in agreement with adsorption kinetic experiments. The half-life time of MIRESORB[TM] was 2.5 h, which was 2.68 times faster than that of GFH. The maximum adsorption capacity of MIRESORB[TM] was 50.38 mg/g, and N_2-sorption isotherms were fit more accurately to the Freundlich model than Langmuir adsorption. Superior arsenic adsorption performance was achieved in MIRESORB[TM] materials under lower pH conditions due to electrostatic interactions between the adsorbent and adsorbate.

The feasibility of MIRESORB[TM] materials to be used for practical applications in water treatment was evaluated by experiments using environmental samples of AMD, using lab-scale column and pilot-plant formats. Using a short EBCT of 11.8 min, the lab-scale column could be operated up to 5840 BV without a breakthrough. Judicious tuning of operating conditions achieved more than 90% arsenic removal efficiency for MIRESORB[TM] materials during pilot-plant operation. Thus, MIRESORB[TM] materials derived from iron-rich acid

mine drainage sludge is a highly efficient and economical material for removing arsenic from wastewater.

References

1. Siddiqui, S.I.; Chaudhry, S.A. Arsenic Removal from Water Using Nanocomposites: A Review. *Curr. Environ. Eng. Contin. Curr. Environ. Manag.* **2017**, *4*, 81–102. [CrossRef]
2. Jomova, K.; Jenisova, Z.; Feszterova, M.; Baros, S.; Liska, J.; Hudecova, D.; Rhodes, C.J.; Valko, M. Arsenic: Toxicity, oxidative stress and human disease. *J. Appl. Toxicol.* **2011**, *31*, 95–107. [CrossRef]
3. World Health Organization. *Guidelines for Drinking-Water Quality: Fourth Edition Incorporating the First Addendum*; World Health Organization: Geneva, Switzerland, 2017.
4. Kwak, J.I.; Nam, S.H.; An, Y.J. Water quality standards for the protection of human health and aquatic ecosystems in Korea: Current state and future perspective. *Environ. Sci. Pollut. Res. Int.* **2018**, *25*, 3108–3119. [CrossRef]
5. Brinkel, J.; Khan, M.H.; Kraemer, A. A Systematic Review of Arsenic Exposure and Its Social and Mental Health Effects with Special Reference to Bangladesh. *Int. J. Environ. Res. Public Health* **2009**, *6*, 1609–1619. [CrossRef]
6. Zheng, Y. Global solutions to a silent poison. *Science* **2020**, *368*, 818–819. [CrossRef]
7. Doyle, P. Environmental Geology. In *Encyclopedia of Geology*; Selley, R.C., Cocks, L.R.M., Plimer, I.R., Eds.; Elsevier: Oxford, UK, 2005; pp. 25–33.
8. Pfeiffer, M.; Batbayar, G.; Hofmann, J.; Siegfried, K.; Karthe, D.; Hahn-Tomer, S. Investigating arsenic (As) occurrence and sources in ground, surface, waste and drinking water in northern Mongolia. *Environ. Earth Sci.* **2015**, *73*, 649–662. [CrossRef]
9. Batsaikhan, B.; Kwon, J.; Kim, K.; Lee, Y.; Lee, J.; Badarch, M.; Yun, S. Hydrochemical evaluation of the influences of mining activities on river water chemistry in central northern Mongolia. *Environ. Sci. Pollut. Res.* **2017**, *24*, 2019–2034. [CrossRef]
10. Kim, S.; Kwon, H.J.; Cheong, H.K.; Choi, K.; Jang, J.Y.; Jeong, W.C.; Kim, D.S.; Yu, S.; Kim, Y.W.; Lee, K.Y.; et al. Investigation on health effects of an abandoned metal mine. *J. Korean Med. Sci.* **2008**, *23*, 452–458. [CrossRef]
11. Hao, L.; Liu, M.; Wang, N.; Li, G. A critical review on arsenic removal from water using iron-based adsorbents. *RSC Adv.* **2018**, *8*, 39545–39560. [CrossRef]
12. Guan, X.; Wang, J.; Chusuei, C.C. Removal of arsenic from water using granular ferric hydroxide: Macroscopic and microscopic studies. *J. Hazard. Mater.* **2008**, *156*, 178–185. [CrossRef]
13. Ma, H.; Zhu, Z.; Dong, L.; Qiu, Y.; Zhao, J. Removal of Arsenate from Aqueous Solution by Manganese and Iron (hydr)oxides Coated Resin. *Sep. Sci. Technol.* **2010**, *46*, 130–136. [CrossRef]
14. Chowdhury, R. Using adsorption and sulphide precipitation as the principal removal mechanisms of arsenic from a constructed wetland—A critical review. *Chem. Ecol.* **2017**, *33*, 560–571. [CrossRef]
15. Kumar, R.; Kang, C.; Mohan, D.; Khan, M.A.; Lee, J.; Lee, S.S.; Jeon, B. Waste sludge derived adsorbents for arsenate removal from water. *Chemosphere* **2020**, *239*, 124832. [CrossRef]
16. Egashira, R.; Tanabe, S.; Habaki, H. Adsorption of heavy metals in mine wastewater by Mongolian natural zeolite. *Proc. Eng.* **2012**, *42*, 49–57. [CrossRef]

17. Zeng, H.; Yu, Y.; Wang, F.; Zhang, J.; Li, D. Arsenic(V) removal by granular adsorbents made from water treatment residuals materials and chitosan. *Colloids Surf. Physicochem. Eng. Asp.* **2020**, *585*, 124036. [CrossRef]

18. Lee, H.; Kim, D.; Kim, J.; Ji, M.; Han, Y.; Park, Y.; Yun, H.; Choi, J. As(III) and As(V) removal from the aqueous phase via adsorption onto acid mine drainage sludge (AMDS) alginate beads and goethite alginate beads. *J. Hazard. Mater.* **2015**, *292*, 146–154. [CrossRef]

19. Demers, I.; Mbonimpa, M.; Benzaazoua, M.; Bouda, M.; Awoh, S.; Lortie, S.; Gagnon, M. Use of acid mine drainage treatment sludge by combination with a natural soil as an oxygen barrier cover for mine waste reclamation: Laboratory column tests and intermediate scale field tests. *Miner. Eng.* **2017**, *107*, 43–52. [CrossRef]

20. Macías, F.; Pérez-López, R.; Caraballo, M.A.; Cánovas, C.R.; Nieto, J.M. Management strategies and valorization for waste sludge from active treatment of extremely metal-polluted acid mine drainage: A contribution for sustainable mining. *J. Clean. Prod.* **2017**, *141*, 1057–1066. [CrossRef]

21. Ko, D.; Lee, J.S.; Patel, H.A.; Jakobsen, M.H.; Hwang, Y.; Yavuz, C.T.; Hansen, H.C.B.; Andersen, H.R. Selective removal of heavy metal ions by disulfide linked polymer networks. *J. Hazard. Mater.* **2017**, *332*, 140–148. [CrossRef]

22. Foo, K.Y.; Hameed, B.H. Insights into the modeling of adsorption isotherm systems. *Chem. Eng. J.* **2010**, *156*, 2–10. [CrossRef]

23. Chwastowski, J.; Bradło, D.; Żukowski, W. Adsorption of Cadmium, Manganese and Lead Ions from Aqueous Solutions Using Spent Coffee Grounds and Biochar Produced by Its Pyrolysis in the Fluidized Bed Reactor. *Materials* **2020**, *13*, 2782. [CrossRef] [PubMed]

24. Song, Y.; Bac, B.H.; Lee, Y.; Kim, M.H.; Kang, I.M. Highly ordered Ge-incorporated akaganeite (β-FeOOH): A tunnel-type nanorod. *Cryst. Eng. Commun.* **2011**, *13*, 287–292. [CrossRef]

25. Chen, X.; Wu, S.; Cao, R.; Tao, J. Preparation and Characterization of Nanosized Hematite Colloids Using Green Vitriol as Ferrum Source. *J. Nanomater.* **2014**, *2014*, 749562. [CrossRef]

26. Ambroz, F.; Macdonald, T.J.; Martis, V.; Parkin, I.P. Evaluation of the BET Theory for the Characterization of Meso and Microporous MOFs. *Small Methods* **2018**, *2*, 1800173. [CrossRef]

27. Baskan, M.B.; Pala, A. Removal of arsenic from drinking water using modified natural zeolite. *Desalination* **2011**, *281*, 396–403. [CrossRef]

28. Mohammad, S.G.; Ahmed, S.M.; Amr, A.; Kamel, A.H. Porous Activated Carbon from Lignocellulosic Agricultural Waste for the Removal of Acetampirid Pesticide from Aqueous Solutions. *Molecules* **2020**, 2339.

29. Yang, J.; Kim, Y.; Park, S.; Baek, K. Removal of As(III) and As(V) using iron-rich sludge produced from coal mine drainage treatment plant. *Environ. Sci. Pollut. Res.* **2014**, *21*, 10878–10889. [CrossRef]

30. Ko, M.; Kim, J.; Lee, J.; Ko, J.; Kim, K. Arsenic immobilization in water and soil using acid mine drainage sludge. *Appl. Geochem.* **2013**, *35*, 1–6. [CrossRef]

31. Rait, R.; Trumm, D.; Pope, J.; Craw, D.; Newman, N.; MacKenzie, H. Adsorption of arsenic by iron rich precipitates from two coal mine drainage sites on the West Coast of New Zealand. *N. Z. J. Geol. Geophys.* **2010**, *53*, 177–193. [CrossRef]

32. Saha, B.; Bains, R.; Greenwood, F. Physicochemical Characterization of Granular Ferric Hydroxide (GFH) for Arsenic(V) Sorption from Water. *Sep. Sci. Technol.* **2005**, *40*, 2909–2932. [CrossRef]

33. Aredes, S.; Klein, B.; Pawlik, M. The removal of arsenic from water using natural iron oxide minerals. *J. Clean. Prod.* **2012**, *29*, 208–213. [CrossRef]

34. Escudero, C.; Fiol, N.; Villaescusa, I.; Bollinger, J. Arsenic removal by a waste metal (hydr)oxide entrapped into calcium alginate beads. *J. Hazard. Mater.* **2009**, *164*, 533–541. [CrossRef] [PubMed]